processes

MDPI

*Article*

# Ice Growth Suppression in the Solution Flows of Antifreeze Protein and Sodium Chloride in a Mini-Channel

**Kazuya Taira [1], Tomonori Waku [2] and Yoshimichi Hagiwara [3,*]**

[1] Division of Mechanophysics, Graduate School of Science and Technology, Kyoto Institute of Technology, Matsugasaki, Sakyo-ku, Kyoto 606-8585, Japan; taira.kazuya@jp.panasonic.com
[2] Faculty of Molecular Chemistry and Engineering, Kyoto Institute of Technology, Matsugasaki, Sakyo-ku, Kyoto 606-8585, Japan; waku1214@kit.ac.jp
[3] Kyoto Institute of Technology, Matsugasaki, Sakyo-ku, Kyoto 606-8585, Japan
* Correspondence: akimd600@tcn.zaq.ne.jp

**Abstract:** The control of ice growth inside channels of aqueous solution flows is important in numerous fields, including (a) cold-energy transportation plants and (b) the preservation of supercooled human organs for transplantation. A promising method for this control is to add a substance that influences ice growth in the flows. However, limited results have been reported on the effects of such additives. Using a microscope, we measured the growth of ice from one sidewall toward the opposite sidewall of a mini-channel, where aqueous solutions of sodium chloride and antifreeze protein flowed. Our aim was to considerably suppress ice growth by mixing the two solutes. Inclined interfaces, the overlapping of serrated interfaces, and interfaces with sharp and flat tips were observed in the cases of the protein-solution, salt-solution, and mixed-solution flows, respectively. In addition, it was found that the average interface velocity in the case of the mixed-solution flow was the lowest and decreased by 64% compared with that of pure water. This significant suppression of the ice-layer growth can be attributed to the synergistic effects of the ions and antifreeze protein on the diffusion of protein.

**Keywords:** ice layer; growth suppression; solution flow; antifreeze protein; sodium chloride; interface morphology; interface velocity

check for updates

**Citation:** Taira, K.; Waku, T.; Hagiwara, Y. Ice Growth Suppression in the Solution Flows of Antifreeze Protein and Sodium Chloride in a Mini-Channel. *Processes* **2021**, *9*, 306. https://doi.org/10.3390/pr9020306

Academic Editor: Ireneusz Zbicinski
Received: 29 December 2020
Accepted: 3 February 2021
Published: 6 February 2021

**Publisher's Note:** MDPI stays neutral with regard to jurisdictional claims in published maps and institutional affiliations.

**Copyright:** © 2021 by the authors. Licensee MDPI, Basel, Switzerland. This article is an open access article distributed under the terms and conditions of the Creative Commons Attribution (CC BY) license (https://creativecommons.org/licenses/by/4.0/).

## 1. Introduction

The suppression of ice growth has been focused on in significant recent research. This suppression is important in numerous fields, including (a) the improvement of storage and transportation of fresh foods; (b) cryotherapy [1]; (c) the preservation of organs for transplantation, using extracorporeal perfusion circuits [2,3]; and (d) cold-energy transportation plants. In cases (a) and (b), the stationary water becomes a supercooled state; in cases (c) and (d), the flowing water becomes a supercooled state. Typically, the levels of ice-growth suppression for flowing water are lower than those for stationary water, because convection heat transfer by the flow causes a non-equilibrium state of thermodynamics. Thus, fewer studies have been performed on ice-growth suppression in flowing water, compared with those in stationary water.

A promising method for controlling ice growth in quiescent water is to add a substance that has the specific control purpose to the water. Antifreeze proteins (AFPs) and antifreeze glycoproteins (AFGPs) are apposite substances that are to control ice growth, as they decrease the temperature at which an ice crystal grows, yet do not significantly change the temperature at which the crystal is stable during melting at extremely low cooling rates. Moreover, a suitable concentration of AF(G)P is considerably less than that of other solutes [4]. This causes the minimum effect of AF(G)P on osmotic pressure.

HPLC6, the major fraction of winter flounder antifreeze protein, has been widely studied among AF(G)Ps discovered to date. The measurements of ice crystal growth

in quiescent solutions of this protein can be categorized according to the cooling rate, $K$, as follows: (1) $K \leq -1$ °C/min (thermodynamically quasi-equilibrium states) and (2) $K > -1.5$ °C/min (thermodynamically non-equilibrium states). In the typical measurements of type (1), the freezing point was evaluated from the temperature at which the growth velocity of a tiny ice crystal in an osmometer exceeded 0.2 μm/s [5]. In the typical measurements of type (2), the morphologies and velocities of the ice/protein solution interfaces [6–10], concentration of HPLC6 [8–10], temperature distribution [8], and average size of the HPLC6 aggregates [10] were obtained for the freezing of AF(G)P solutions in narrow spaces. The ice-growth velocity in References [6–10] was in the range of 2–20 μm/s. It was thought in these references that serrated interfaces were produced by the adsorption of AF(G)P and the approach of AFP aggregates or a high-concentration region of AFP to the interfaces. The concentration distributions of an anion and AFP in the mixed solution were changed by the other solute, which was a possible reason for the low values of temperature at the ice/solution interface [9]. In addition, the ice nucleation rate was obtained for an HPLC6 solution in a glass tube [11].

It has not yet been confirmed whether these valid findings hold in the situation where the solution flows along the ice surfaces inside channels. Moreover, the experimental results for such flows are limited. It was demonstrated that the pressure drop for the ice slurry flow with HPLC6 (i.e., HPLC6-solution flow with ice particles) in a pipe with a 6 mm inner diameter was greater than that for water flow in the identical pipe [12]. The growth of seed crystals in the direction of the c-axis in the quiescent solution, in addition to the crystals being transported in the central region of the flow, was also observed. Takeshita et al. [13] demonstrated that the ice-growth inhibition by HPLC6 decreased in flowing solutions, compared with that in quiescent solutions in a mini-channel. They also determined that ultrafiltration after preheating the HPLC6 solution enhanced the ice-growth inhibition in a specific case. To the best of our knowledge, there are no reports on the effects of AFP-solution flows on ice layers growing from the channel's inner walls. These ice layers occur in the aforementioned fields (c) and (d). In addition, the effects of AFP solution flow cannot be predicted well from the findings of ice slurry flows, because the relative velocities of the solution flowing to the ice layers are considerably greater than those of the ice particles in the slurry flows. Thus, experimental results are required.

Hence, in this study, we perform experiments on the growth of ice layers on the sidewall of a mini-channel for an HPLC6 solution flow. We force the ice to grow from a specific position in the channel, to guarantee reproducibility without loss of generality. Although the bulk mean velocity in this mini-channel is considerably less than that in the aforementioned fields (c) and (d), our findings are expected to contribute to the elucidation of the early stage of ice-layer growth in these fields.

## 2. Materials and Methods

### *2.1. Materials*

HPLC6 has a molecular weight of 3242 Da and consists of 37 amino acids, whose sequence is shown as follows: DTASDAAAAAALTAANAKAAAELTAANAAAAAAATAR (A = alanine, D = aspartic acid, E = glutamic acid, K = lysine, L = leucine, N = asparagine, R = arginine, S = serine, and T = threonine). Its secondary structure is an α-helix. The axial length and diameter of HPLC6 are approximately 5 and 1 nm, respectively [14]. Four threonine residues are positioned at virtually identical distances on one line, parallel to the helical axis. The distance between the neighboring threonine is virtually identical to the distance between the oxygen atoms on the bi-pyramidal facets of the ice crystals that were observed in the solution of HPLC6. Thus, the following hypothesis was discussed: The hydrogen atoms of the threonine were bonded permanently to the oxygen atoms on the bi-pyramidal facets in the ice crystal, and thus the bonding of water molecules to the facets was prevented [5]. Discussions on the alanine-rich surfaces of HPLC6 were also conducted in the ice-growth inhibition mechanism [15,16]. HPLC6 can be synthesized by

using chemical compounds. We purchased synthetic HPLC6 from Operon Biotechnology Inc. (Tokyo, Japan) and Life Technologies Corporation (Carlsbad, CA, USA).

### *2.2. Apparatus*

The apparatus consisted of an inverted microscope (Nikon ECLIPSE Ti-E), monochrome charge-coupled device (CCD) video camera (Hamamatsu Photonics, ORCA-ER), syringe pump (HARVARD APPARATUS, MA170-2205), and cooling section. The apparatus was arranged in a temperature-controlled room maintained at 5.5 ± 0.9 °C.

### *2.3. Mini-Channel*

Figure 1 displays the mini-channel. The channel was made of a large glass slide of thickness 1, width 52, and length 76 mm and a grooved polydimethylsiloxane (PDMS) plate of thickness 1, width 30, and length 70 mm. This plate was glued to the glass slide. The dimensions of the channel were depth 0.30 mm, width 2.0 mm, and length 60 mm. The equivalent diameter, *D*, was 0.52 mm. Silicone tubes were attached to access port A (channel entrance) and access port B (channel exit). The tube attached to access port A was connected to a syringe pump, to introduce the solution into the channel. Two microchannels extended perpendicular to the sidewalls of the mini-channel. The dimensions of the microchannels were depth 0.30 mm and width 0.10 mm. One of the microchannels was used for freezing water, to promote ice growth from a specific location on the sidewall of the mini-channel. The other microchannel, which extended to the edge of the PDMS chip, was closed with glue. The Cartesian coordinates were arranged as follows: The *X*-axis was in the ice-growth direction in the viewing area, the *Y*-axis was in the solution-flow direction, and the *Z*-axis was in the viewing direction.

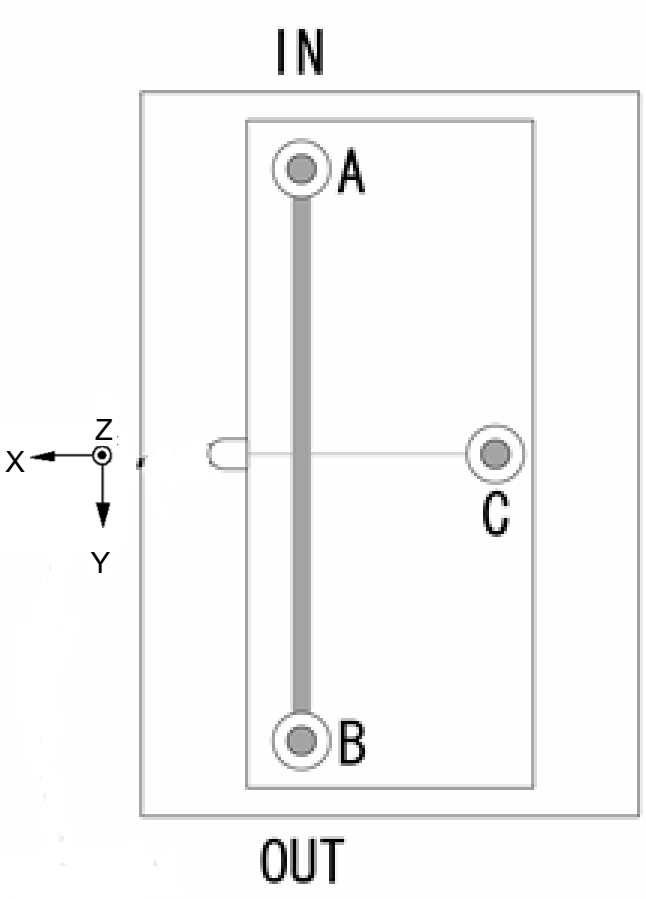



**Figure 1.** Top view of mini-channel.

As shown in Figure 2, part of the glass slide was fixed onto a U-shaped acrylic–resin table. This table was mounted on the left-hand side of the microscope bench. A heat sink (cold plate P-400S, Takagi Mfg. Co. Ltd., Hitachinaka, Japan) was mounted on the right-hand side of the bench. The ethylene glycol coolant flowed through this heat sink. The temperature of the coolant was controlled, using a constant-temperature liquid bath (BB301, Yamato Scientific Co. Ltd., Tokyo, Japan). On the top surface of the heat sink, a 40 mm square Peltier device was fixed such that the heat-generation side of the device was cooled by the heat sink. The input voltage to the device was regulated with a controller (SDC31, Azbil Co., Tokyo, Japan), to obtain a predetermined temperature gradient. The accuracy of the controller was ±0.05 °C. A copper plate of the same size was fixed on the heat-absorption side of the device, with thermally conductive grease 2 mm in thickness. The device and copper plate were arranged such that the diagonal of the plate was along the *X*-axis. A small area near the forward corner of the plate in the X-direction was coated with identical grease. On the microscope bench, we carefully slid the U-shaped table with the mini-channel, toward the heat sink, until the forward corner of the copper plate reached the center of the glass slide. We confirmed that the small gap between a part of the glass surface and copper plate was completely filled with the grease. Consequently, water in access port C and in the microchannel 10 mm in length was directly cooled with the device through the copper plate and grease layers. Owing to the arrangement of cooling device, the ice-layer width in the flow direction was restricted to less than 30% of the mini-channel length. Thus, an increase in the pressure and a change in the flow rate by the ice growth along the sidewall were reduced.

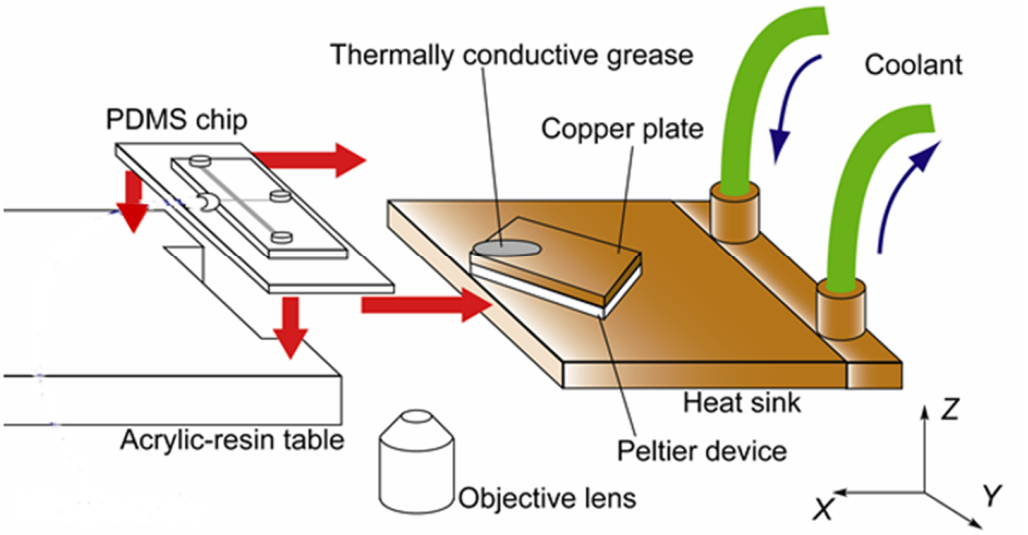



**Figure 2.** Arrangement of mini-channel on the bench of microscope.

### *2.4. Experimental Condition*

Table 1 lists the concentration conditions of the solutions. Cases 1, 2, 3, and 4 are deionized (DI) water, a sodium chloride solution, a dilute HPLC6 solution, and a mixed solution of sodium chloride and HPLC6, respectively. All solutions were prepared with DI water. The concentration of HPLC6 was 0.25 mg/mL, which corresponded to 0.080 mM. The concentration of sodium chloride was 0.45 wt%, which corresponded to 77 mM. Thus, the molar concentration of the sodium chloride was approximately 100 times greater than the molar concentration of the HPLC6.

**Table 1.** Concentration condition of solutions.

| Case | 1 | 2 | 3 | 4 |
|---|---|---|---|---|
| *HPLC6* (mg/mL) | 0 | 0 | 0.25 | 0.25 |
| *NaCl* (wt%) | 0 | 0.45 | 0 | 0.45 |

The flow rates of the water and solutions were set at 10 μL/min. The bulk mean velocity before the ice-layer growth, $V$, was 0.28 mm/s. Because the kinematic viscosity of water, $\nu$, is 1.673 $mm^2/s$ at 2 °C, the Reynolds number, $VD/\nu$, was 0.087. This Reynolds number is in the range of the liquid flow in arterioles in the human body [17] and xylem vessels in plants [18]. It was found, in a previous study by our group [19], that the average growth velocity of the ice layer for the HPLC6-solution flow in an identical mini-channel did not depend on the flow rate. In this study, the deviation of the growth velocity from its averaged value was only 5%, −11%, and 5% with the change in the flow rate of 0, 10, and 20 μL/min, respectively.

The predetermined temperature gradient of the Peltier device was set to –6.0 °C/min. This temperature gradient was less than that of cryotherapy [1] and in the optimal range of the cryopreservation of cells [20].

The image-capturing conditions are presented in Table 2. We allocated lines parallel to the sidewall with the outlet of the microchannel at every 50 pixels (0.117 mm) on the captured images. The interface velocity was evaluated from the following two images and time difference between the two instants for these images: an image in which the most advanced point of the interface had reached a line, and another image in which this point had reached the adjacent line. The margin of error for the interface velocity did not exceed 10% and decreased with a decrease in the velocity.

**Table 2.** Image-capturing conditions.

| | |
|---|---|
| Magnification | ×5 |
| Binning | 2 × 2 |
| Pixel number | 672 × 512 |
| Area size ($\mu m^2$) | 1572 × 1198 |
| Pixel resolution ($\mu m^2$) | 2.34 × 2.34 |
| Frame rate (fps) | 1 |
| Exposure time (s) | 0.05 |

## 3. Results

### *3.1. Interface Morphology*

Figure 3 displays typical images for each case in early stages. In each image, the sidewall of the mini-channel and outlet of the microchannel are indicated on the right-hand side. The ice grew in the left direction; the liquid flow direction was downward on the images. In the cases of the water and AFP-solution flows, the ice layer instantaneously formed along the sidewall when the ice crystal entered the mini-channel from the outlet of the microchannel, as indicated in Figure 3a,c, respectively. In the cases of the salt-solution and mixed-solution flows, conversely, the ice crystals grew preferentially in the X-direction (perpendicular to the flow direction), immediately after it entered the mini-channel, as indicated in Figure 3b,d, respectively. The reason for the difference in the ice-growth direction in early stages is discussed in the Discussion section.

Figure 4 displays typical images for each case in ice-layer growth stages. In the case of the DI water flow in Figure 4a, two lines can be observed on the left-hand side of the image. We changed the location of the focal plane by moving the microscope stage in the Z-direction, and confirmed that the leftmost line (Line A) indicates the location of the interface at the glass slide surface, whereas the other line (Line B) indicates the interface at

the PDMS chip surface in the mini-channel. Thus, the interface was inclined. The angle ($\theta$) between the interface and ($Y$, $Z$) plane can be estimated from the following equation:

$$\theta = \tan^{-1}(l_X/d), \quad (1)$$

where $l_X$ is the distance between the two lines in the X-direction, and $d$ (= 0.30 mm) is the depth of the mini-channel. The value of $\theta$ was 21°, because the distance $l_{Xwater}$ was 0.115 mm. Moreover, it was found, by analyzing other images, that $\theta$ was independent of the time and interface location, except for the initial stage of ice-layer growth in the mini-channel. This is because the location of the Peltier device was distant and low from the mini-channel.

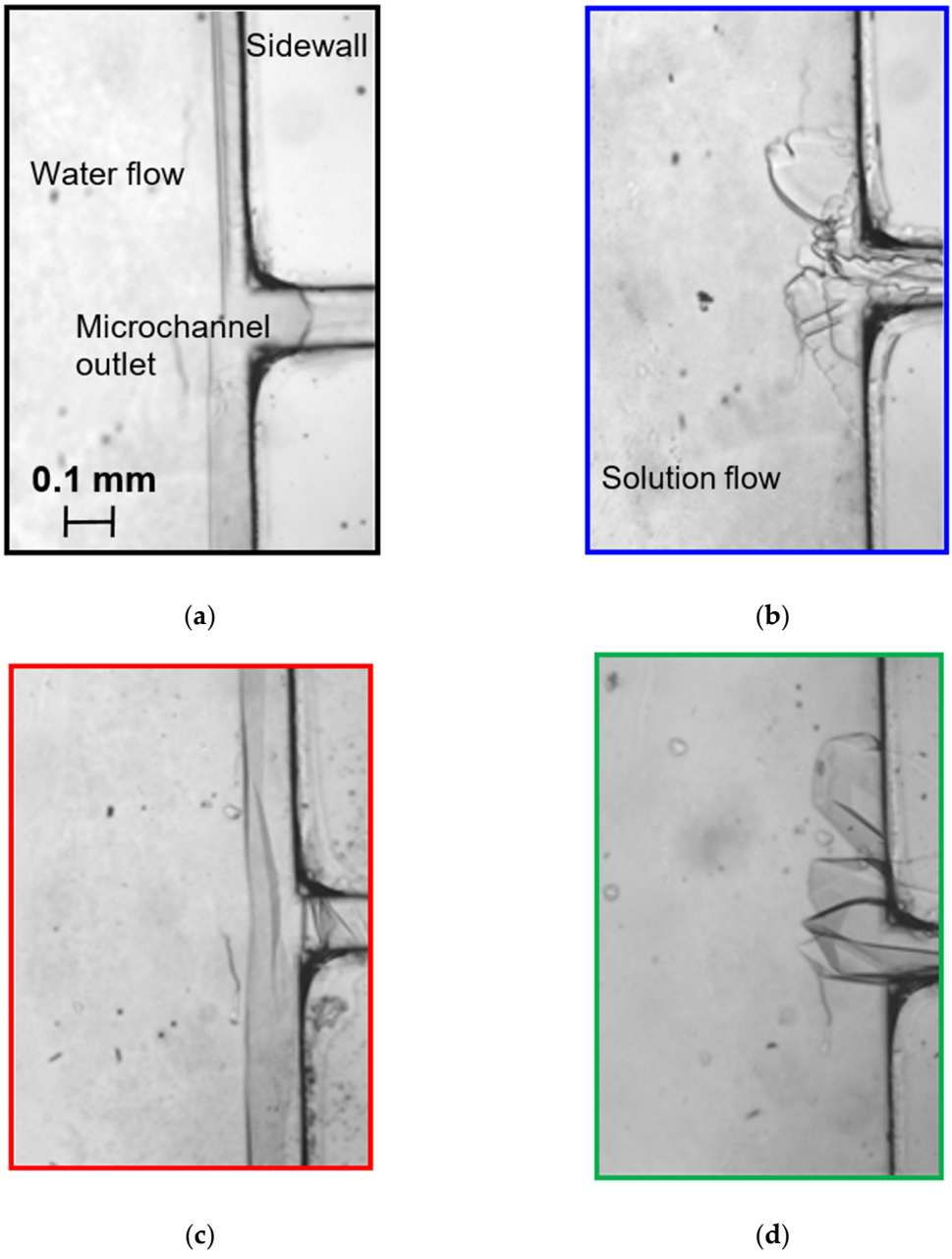



**Figure 3.** Typical images of ice/liquid flow interfaces in early stages: (**a**) deionized (DI) water flow, (**b**) salt-solution flow, (**c**) HPLC6-solution flow, and (**d**) mixed-solution flow.

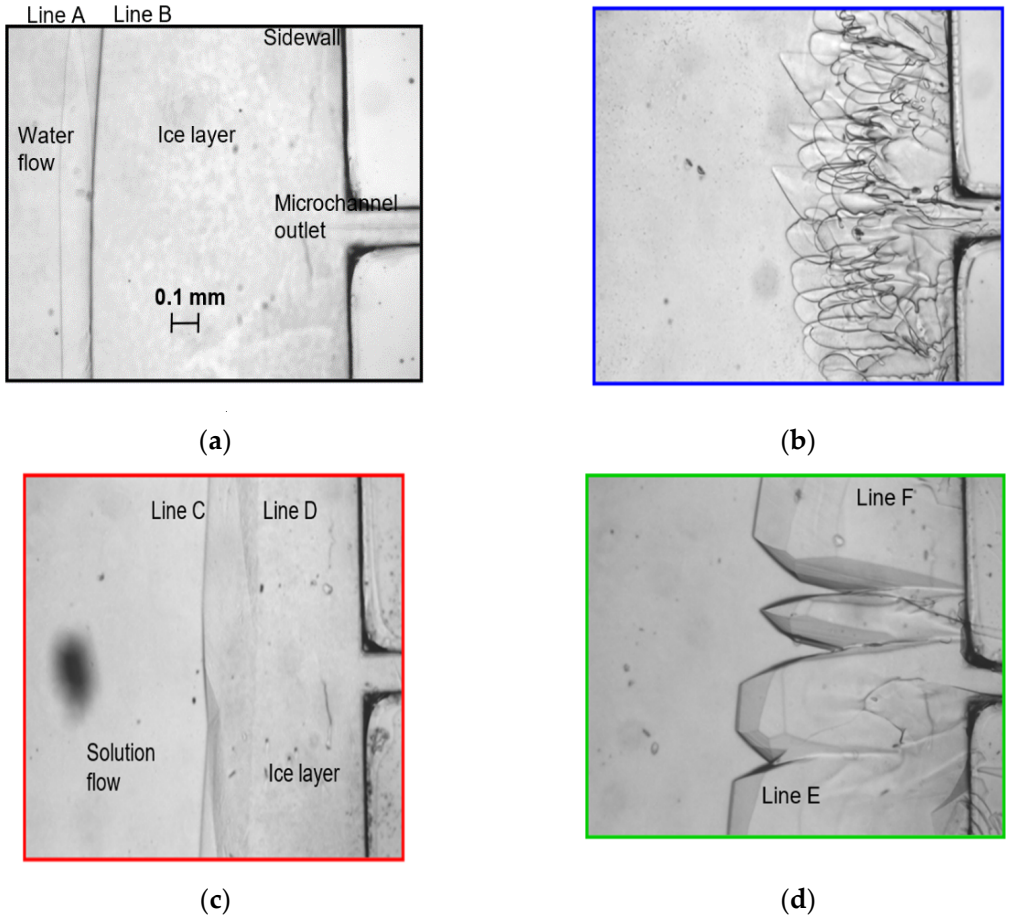



**Figure 4.** Typical images of ice/liquid flow interfaces in ice-layer growth stages: (**a**) DI water flow, (**b**) salt-solution flow, (**c**) HPLC6-solution flow, and (**d**) mixed-solution flow.

In the case of the salt-solution flow, four or five thin layers of pectinated interfaces overlap in the Z-direction, as indicated in Figure 4b. The most advanced interface with a sharp tip was located in the thin layer adjacent to the surface of the glass slide. Conversely, interfaces with numerous finger-like round tips were located in each of the other thin layers. These interfaces of different types were similar to the interfaces observed for the unidirectional freezing of the salt solution in a narrow space between two cover glasses [9,21] (also refer to Appendix A).

In the case of the HPLC6-solution flow, two lines, C and D, can be observed in Figure 4c. Line C indicates the location of the interface on the glass slide surface, whereas Line D indicates the location of the interface on the PDMS chip surface. As the distance between these two lines is wider than that between Lines A and B, this interface is inclined further than the ice/water interface displayed in Figure 4a. This is consistent with the serrated interface observed for the unidirectional freezing of an HPLC solution in a narrow space [8,9,22]. The angle $\theta$ was 36°, because the distance between Lines C and D in Equation (1), $l_{XHPLC6}$, was 0.215 mm. The difference between this angle and the angle for the water flow is 15°, which is equal to the angle of the specific pyramidal facet of the ice crystals in the HPLC6 solution [23,24]. Thus, this interface is considered to have resulted from the adsorption of AFP.

Several short lines can be observed on the interface in Figure 4c. This indicates that the inclined interface was not smooth; rather, it had shallow dents locally. It was observed from successive images that, as the ice layer grew, these shallow dents appeared to move gradually in the streamwise direction; however, the distance between the Lines C and D remained unchanged with time. This is discussed in the next section.

In the case of the flow of the mixed solution, both a narrow part with a sharp tip and wide parts with flat tips can be observed on the interface, as indicated in Figure 4d. The narrow part is similar to the interface observed for the unidirectional freezing of a mixed solution in the narrow space between two cover glasses [21]. In addition, the distance between the two adjacent tips is greater than that for the other solution flow cases, which is consistent with the results for unidirectional freezing [21] (refer to Appendix A). Conversely, the tips of these wide parts are similar to the interface of the HPLC6-solution flow displayed in Figure 4c. Thus, it is expected that the local AFP concentration was high around the sharp tip and low near the flat tips. Moreover, multiple lines, such as Lines E and F, can be observed in all parts of the crystal. This indicates that the interface consisted of several small facets with different inclined angles. The inclined angle $\theta$ increased with an increase of the height from the surface of the glass slide. This could be caused by the HPLC6 concentration increasing near the PDMS surface by the ions. This is discussed in the Discussion section.

### 3.2. Interface Velocity

Figure 5 displays the interface velocity in the X-direction as a function of the number of pixels or the distance from the sidewall in the following runs: (1) two runs in the case of water flow, (2) two runs in the case of salt-solution flow, (3) three runs in the case of HPLC6-solution flow, and (4) two runs in the case of mixed-solution flow. In each of the solution cases, the lines are similar. Thus, reproducibility was confirmed.

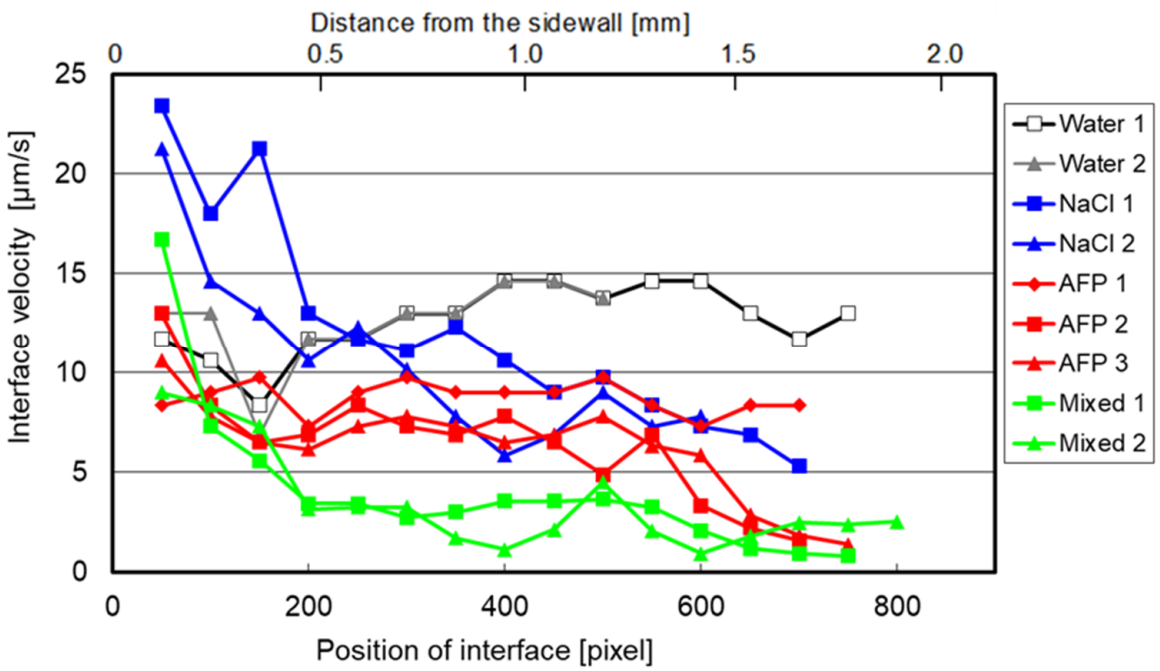



**Figure 5.** Interface velocity as function of distance from sidewall.

In the cases of the water and AFP-solution (run #1) flows, the interface velocity did not change significantly with the location. In these cases, the ice layer instantaneously formed along the sidewall in early stages (refer to Figure 3a,c). In the cases of the other solution flows, conversely, the interface velocity decreased remarkably with time, until the interfaces arrived at a position of 0.648 mm (200 pixels) from the sidewall. This is the results of the preferential growth of ice crystals, as indicated in Figure 3b,d. After the arrival of the interface at 0.648 mm, the interface velocity decreased gradually as the ice layer grew.

We calculated the overall interface velocity, $\overline{U_i}$ $(i = 1, 2, 3, 4)$, for each case, using the results displayed in Figure 5. The overall interface velocities and their ratios are listed in Table 3. The overall interface velocities for the salt-solution, HPLC6-solution, and mixed -solution flows were 10%, 44%, and 64%, respectively, less than the overall interface velocity of the water flow. This is consistent with the decrease in the temperature at the interface in the unidirectional freezing of identical solutions [9,21]. If the ions and HPLC6 act independently in the mixed solution, the ratio $\overline{U_4}/\overline{U_1}$ should be $0.90 \times 0.56 = 0.50$, whereas the ratio is only 0.36, as presented in Table 3. That is, the overall interface velocity for the mixed-solution flow was considerably lower than expected, using the overall interface velocities for the single-component solution flows. This clearly confirms that the two solutes interacted with each other in the mixed-solution flow. This is similar to the synergistic effects of AFP and ionic compounds on the decrease in the temperature at the interface in the unidirectional freezing of identical solutions [9,21] and on the decrease in the freezing point in the thermodynamically quasi-equilibrium states in osmometers [25,26].

**Table 3.** Overall interface velocities and their ratios.

| Case | 1 (Water) | 2 (Salt Solution) | 3 (AFP Solution) | 4 (Mixed Solution) |
|---|---|---|---|---|
| $\overline{U_i}$ $(i = 1, 2, 3, 4)$ (μm/s) | 12.6 | 11.3 | 7.1 | 4.6 |
| $\overline{U_i}/\overline{U_1}$ $(i = 1, 2, 3, 4)$ | 1 | 0.90 | 0.56 | 0.36 |

AFP, antifreeze protein.

## 4. Discussion

Generally, as an ice crystal grows and, thus, its surface becomes wider in water or aqueous solution in a limited space, the ice growth is attenuated. This is because the amount of latent heat of fusion increases with an increase in the ice surface area. Thus, a period necessary for the dissipation of the latent heat becomes longer. This is the reason for the decreases in the interface velocities in early stages shown in Figure 5.

The freezing point of the sodium chloride solution is −0.28 °C. The freezing point of the HPLC6 solution is in the range of −0.079 to −0.18 °C, based on the experimental results in [4,5]. The freezing point of the mixed solution is estimated to be lower than −0.36 °C, by taking account of the synergistic effect of solutes [25,26]. The ion concentration around the ice crystals shown in Figure 3b,d increased with time. This is based on the following findings of the experiments on unidirectional freezing: The ion concentration was highest at the ice/solution interface and decreased with the distance from the interface at any instant [9,27], and it increased with an ice growth at any location from the interface unless it was low enough [27]. Thus, the supercooled state was maintained in a region adjacent to the cold sidewall. This is the reason for the restricted areas of ice and the high interface velocities in early stages, in the cases of the salt-solution flow and mixed-solution flow.

The difference in the interface shape discussed for Figure 4 is assumed to be caused by the diffusion of the solutes. Based on the results reported by Inglis et al. [28], the diffusion coefficient of HPLC6, $D_{HPLC6}$, can be estimated by using the following empirical equation:

$$D_{HPLC6}/D_0 = -0.028c + 1, \quad (2)$$

where $D_0 = 0.670 \times 10^{-10}$ [m$^2$/s] is the infinite dilute diffusion coefficient, and $c$ [mM] is the concentration of HPLC6. Thus, $D_{HPLC6}$, in the present study ($c$ = 0.080 [mM]), is equal to $0.668 \times 10^{-10}$ [m$^2$/s]. The diffusion coefficients of sodium ion and chloride ion in water are, respectively, $D_{Na} = 1334 \times 10^{-9}$ [m$^2$/s] and $D_{Cl} = 2032 \times 10^{-9}$ [m$^2$/s] [29]. Thus, $D_{HPLC6}$ is 5% of $D_{Na}$ and 3% of $D_{Cl}$, approximately. This indicates that the diffusion of HPLC6 molecules across the streamlines is considerably lower than the diffusion of ions across the streamlines. It can be surmised that virtually all of the HPLC6 molecules were transported downstream and that the number of HPLC6 molecules adsorbed to the ice surface increased gradually with time. Thus, the interface for the HPLC6-solution flow in

the early period, indicated in Figure 3c, is similar to that for the water flow. Moreover, it can be surmised that numerous HPLC6 molecules, transported along the inclined surface, produced more inclined surfaces, owing to their gradual adsorption. During this process, the shallow dents of the interface appeared, owing to the local fluctuation of the ice growth, which could have been triggered by the marginally high concentration regions of the AFP. These marginally high concentration regions were transported by the flow before the slow diffusion of the AFP minimized the concentration fluctuation, as the diffusion coefficient of the AFP was extremely low. The interface morphology displayed in Figure 4c and interface velocity in Figure 5 can be reasonably explained by this scenario.

When an ice crystal, such as that shown in Figures 3b and 4b, grew in the mini-channel, not only the ion concentration around the interface increased but also the ions in the flow diffused toward the interface simultaneously, even though the flow was detoured by the ice crystals. Thus, the ion concentration increased where the detoured flow approached the ice surface, facing basically upstream. This high concentration of ions attenuated the ice growth locally. Consequently, the ice crystals grew perpendicularly to the flow in the early stage. As the ice crystals grew, the detoured flow was detached from the sidewall, and the stagnant regions of flow became wider along the sidewall. These thoughts can explain the interfaces displayed in Figures 3b and 4b and the continuous decrease in the interface velocity in Figure 5.

Regarding the mixed solution, we discussed the possible mechanism of the enhancement of the decrease in the temperature at the interface as follows, using the measured concentrations of the ion and HPLC6 in the unidirectional freezing in our previous study [9]. The diffusion of a large number of ions in the ice-growth direction produced the diffusion of the HPLC6 molecules from the bottom-edge regions to the near-tip regions of the serrated interface. The diffused AFP increased its concentration in the region adjacent to the tips. This increase in the HPLC6 concentration contributed to the enhancement of the decrease in the temperature at the interface. In the present study, the diffusion of ions across the streamline transported a large number of HPLC6 molecules toward the cold sidewall. Throughout the ice-growth process, some HPLC6 molecules were adsorbed to the surfaces of the finger-like parts of the crystals and produced quartz-like parts of the ice crystals. Other molecules formed their high-concentration regions [8] and formed narrow liquid regions between the ice crystals, as indicated in Figures 3d and 4d. Moreover, as the ice layer thickened and the amount of diffused HPLC6 increased, the replacement of the ions by the adsorbable HPLC6 molecules caused the formation of multiple inclined parts of the interface, as indicated in Figure 4d. Owing to these remarkable effects of HPLC6 on the interface, the interface velocity decreased, as indicated in Figure 5. Therefore, the growth of the ice layer along the cold sidewall can be significantly attenuated by the flow of a dilute mixed solution of AFP and salt, owing to the synergistic effects of these two solutes.

## 5. Conclusions

We performed experiments on the growth of ice layers on the sidewall of a mini-channel for the flows of water, salt solution, HPLC6 solution, and mixed solution. We measured the interface morphology and interface velocity by analyzing the captured images. The main conclusions obtained are as follows:

(1) The overlapping of serrated interfaces, the inclined interfaces, and the interfaces with sharp and flat tips were observed in the cases of the salt-solution, protein-solution, and mixed-solution flows, respectively.
(2) The average interface velocity in the case of the mixed-solution flow was the lowest, and it decreased by 64%, compared with that of water flow.
(3) The synergistic effects of the ions and antifreeze protein, which were discussed concerning the ice growth in the osmometer and unidirectional freezing, were confirmed in the case of ice growth along the mixed-solution flow in the mini-channel.

**Author Contributions:** Conceptualization, K.T. and Y.H.; methodology, K.T.; validation, K.T. and Y.H.; formal analysis, K.T. and Y.H.; investigation, K.T.; resources, Y.H.; data curation, K.T.; writing—original draft preparation, Y.H.; writing—review and editing, K.T. and T.W.; visualization, Y.H.; supervision, Y.H.; project administration, Y.H.; funding acquisition, Y.H. and T.W. All authors have read and agreed to the published version of the manuscript.

**Funding:** This research was funded by JSPS KAKENHI, grant numbers JP24360081 and JP19K12800.

**Institutional Review Board Statement:** "Not applicable" for studies not involving humans or animals.

**Informed Consent Statement:** "Not applicable" for studies not involving humans.

**Data Availability Statement:** The data presented in this study are available on request from the corresponding author.

**Acknowledgments:** The authors thank Y. Onishi and Y. Nakagawa, former graduate students at Kyoto Institute Technology, for their help.

**Conflicts of Interest:** The authors declare no conflict of interest.

## Appendix A

In our previous study [21], we performed experiments on the unidirectional freezing of solutions of HPLC6, NaCl, and their mixture. The space for the solutions was $50 \times 20 \times 0.02$ mm$^3$ between two cover glasses. The apparatus and method were identical to those in the present study, except for the following conditions: The concentration of the HPLC6 was 0.125 mg/mL, interface velocity was 6.0 μm/s with an error of ±15%, size of the image-capturing area was $392 \times 299$ μm$^2$, pixel resolution was $0.292 \times 0.292$ μm$^2$, and room temperature was approximately 8 °C. Figure A1 displays typical images of the salt solution and mixed solution of salt and HPLC6.

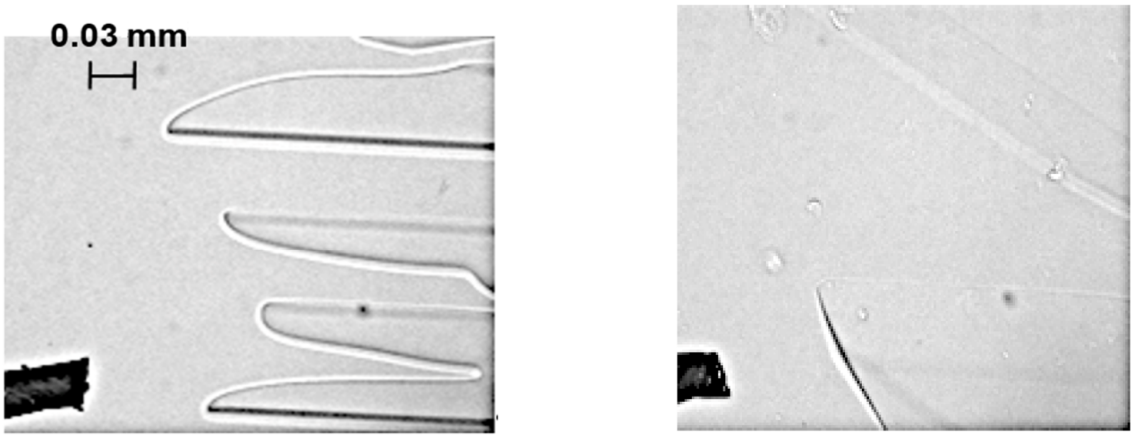



**Figure A1.** Typical images of ice/solution interfaces: (**a**) salt solution and (**b**) mixed solution. The black areas show the shadows of micro thermocouples.

## References

1. Shitzer, A. Cryosurgery: Analysis and experimentation of cryoprobes in phase changing media. *J. Heat Transf.* **2011**, *133*, 011005. [CrossRef]
2. Berendsen, T.A.; Bruinsma, B.G.; Puts, C.F.; Saeidi, N.; Usta, O.B.; Uygun, B.E.; Izamis, M.-L.; Toner, M.; Yarmush, M.L.; Uybun, K. Supercooling enables long-term transplantation survival following 4 days of liver preservation. *Nat. Med.* **2014**, *20*, 790–793. [CrossRef]
3. Ishikawa, J.; Oshima, M.; Iwasaki, F.; Suzuki, R.; Park, J.; Nakao, K.; Matsuzawa-Adachi, Y.; Mizutsuki, T.; Kobayashi, A.; Abe, Y.; et al. Hypothermic temperature effects on organ survival and restoration. *Sci. Rep.* **2015**, *5*, 09563. [CrossRef] [PubMed]

4. Haymet, A.D.J.; Ward, L.G.; Harding, M.M. Winter flounder "antifreeze" proteins: Synthesis and ice growth inhibition of analogues that probe the relative importance of hydrophobic and hydrogen-bonding interactions. *J. Am. Chem. Soc.* **1999**, *121*, 941–948. [CrossRef]
5. Chao, H.; Houston, M.E., Jr.; Hodges, R.S.; Kay, C.M.; Sykes, B.D.; Loewen, M.C.; Davies, P.L.; Sönnichsen, F.D. A diminished role for hydrogen bonds in antifreeze protein binding to ice. *Biochemistry* **1997**, *36*, 14652–14660. [CrossRef]
6. Furukawa, Y.; Inohara, N.; Yokoyama, E. Growth patterns and interfacial kinetic supercooling at ice/water interfaces at which anti-freeze glycoprotein molecules are adsorbed. *J. Cryst. Growth* **2005**, *275*, 167–174. [CrossRef]
7. Butler, M.F. Freeze concentration of solutes at the ice/solution interface studied by optical interferometry. *Cryst. Growth Des.* **2002**, *2*, 541–548. [CrossRef]
8. Hagiwara, Y.; Yamamoto, D. Temperature distribution and local heat flux in the unidirectional freezing of antifreeze-protein solution. *Int. J. Heat Mass Transf.* **2012**, *55*, 2384–2393. [CrossRef]
9. Hagiwara, Y.; Aomatsu, H. Supercooling enhancement by adding antifreeze protein and ions to water in a narrow space. *Int. J. Heat Mass Transfer* **2015**, *86*, 55–64. [CrossRef]
10. Miyamoto, T.; Nishi, N.; Waku, T.; Tanaka, N.; Hagiwara, Y. Effects of short-time preheating on ice growth in antifreeze polypeptides solutions in a narrow space. *Heat Mass Transf.* **2018**, *54*, 2415–2424. [CrossRef]
11. Wilson, P.W.; Heneghan, A.F.; Haymet, A.D.J. Ice nucleation in nature: Supercooling point (SCP) measurements and the role of heterogeneous nucleation. *Cryobiology* **2003**, *46*, 88–98. [CrossRef]
12. Grandum, S.; Yabe, A.; Nakagomi, K.; Tanaka, M.; Takemura, F.; Kobayashi, Y.; Ikemoto, M.; Frivik, P. Investigation of the characteristics of ice slurry containing antifreeze protein for ice storage applications. *Trans. Jpn. Soc. Mech. Ser. B* **1997**, *63*, 1770–1776. (In Japanese) [CrossRef]
13. Takeshita, Y.; Waku, T.; Wilson, P.W.; Hagiwara, Y. Effects of winter flounder antifreeze protein on the growth of ice particles in an ice slurry flow in mini-channels. *Biomolecules* **2019**, *9*, 70. [CrossRef]
14. Knight, C.A.; Cheng, C.C.; DeVries, A.L. Adsorption of $\alpha$-helical antifreeze peptides on specific ice crystal surface planes. *Biophys. J.* **1991**, *59*, 409–418. [CrossRef]
15. Davies, P.L.; Baardsnes, J.; Kuiper, M.J.; Walker, V.K. Structure and function of antifreeze proteins. *Phil. Trans. R. Soc. Lond. B* **2002**, *357*, 927–935. [CrossRef]
16. Jorov, A.; Zhorov, B.S.; Yang, D.S.C. Theoretical study of interaction of winter flounder antifreeze protein with ice. *Protein Sci.* **2004**, *13*, 1524–1537. [CrossRef]
17. Caro, C.G.; Pedley, T.I.; Seed, W.A. Mechanics of the circulation. In *Cardiovascular Physiology*; Guyton, A.C., Ed.; Medical and Technical Publishers: London, UK, 1974; Chapter 1.
18. Ellerby, D.J.; Ennos, A.R. Resistances to fluid flow of model xylem vessels with simple and scalariform perforation plates. *J. Exp. Bot.* **1998**, *49*, 979–985. [CrossRef]
19. Onishi, Y. An Experimental Study on Mechanism of Ice Growth Inhibition of Antifreeze Protein in Flowing Water in Mini-Channel. Master Thesis, Kyoto Institute of Technology, Kyoto, Japan, 21 February 2012. (In Japanese).
20. Baust, J.B.; Gao, D.; Baust, J.M. Cryopreservation: An emerging paradigm change. *Organogenesis* **2009**, *5*, 90–96. [CrossRef]
21. Hagiwara, Y.; Yamamoto, D. Cooperative effect of winter flounder antifreeze protein and ions on the unidirectional freezing of their solution in a narrow space. In *Physics and Chemistry of Ice 2010*; Hokkaido University Press: Sapporo, Japan, 2011; pp. 313–319.
22. Hagiwara, Y.; Sakurai, R.; Nakanishi, R. Temperature of the solution of winter flounder antifreeze protein near ice surfaces in a narrow space. *J. Cryst. Growth* **2010**, *312*, 314–322. [CrossRef]
23. Madura, J.D.; Baran, K.; Wierzbicki, A. Molecular recognition and binding of thermal hysteresis proteins to ice. *J. Mol. Recognit.* **2000**, *13*, 101–113. [CrossRef]
24. Hagiwara, Y. Peculiar freezing fronts of solutions for antifreeze protein or antifreeze polypeptide in a narrow space (in Japanese). *J. Jpn. Assoc. Cryst. Growth* **2018**, *45*, 2-03.
25. Evans, R.P.; Hobbs, R.S.; Goddard, S.V.; Fletcher, G.L. The importance of dissolved salts to the in vivo efficacy of antifreeze proteins. *Comp. Biochem. Physiol. Part A* **2007**, *148*, 556–561. [CrossRef] [PubMed]
26. Kristiansen, E.; Pedersen, S.A.; Zachariassen, K.E. Salt-induced enhancement of antifreeze protein activity: A salting-out effect. *Cryobiology* **2008**, *57*, 122–129. [CrossRef] [PubMed]
27. Nagashima, K.; Furukawa, Y. Time development of a solute diffusion field and morphological instability on a planar interface in the directional growth of ice crystals. *J. Cryst. Growth* **2000**, *209*, 167–174. [CrossRef]
28. Inglis, S.R.; McGann, M.J.; Price, W.S.; Harding, M.M. Diffusion NMR studies on fish antifreeze proteins and synthetic analogues. *FEBS Lett.* **2006**, *580*, 3911–3915. [CrossRef]
29. Vanýsek, P. Ionic conductivity and diffusion at infinite dilution. In *CRC Handbook of Chemistry and Physics, Internet Version 2005*; Lide, D.R., Ed.; CRC Press: Boca Raton, FL, USA, 2005; Section 5; pp. 93–94. Available online: http://www.hbcpnetbase.com (accessed on 29 December 2020).